International Journal of Microwave and Wireless Technologies, 2017, 9(3), 613–620.
doi:10.1017/S1759078716000076

RESEARCH PAPER

Neurospectral computation for the resonant characteristics of microstrip patch antenna printed on uniaxially anisotropic substrates

LAMIA BARKAT[1], SAMI BEDRA[2], TAREK FORTAKI[1] AND RANDA BEDRA[1]

Modeling and design of rectangular microstrip patch printed on isotropic or anisotropic substrate are accomplished in this paper. The use of spectral domain method in conjunction with artificial neural networks (ANNs) to compute the resonant characteristics of rectangular microstrip patch printed on isotropic or anisotropic substrates. The moment method implemented in the spectral domain offers good accurateness, but its computational cost is high owing to the evaluation of the slowly decaying integrals and the iterative nature of the solution process. The paper introduces the electromagnetic knowledge combined with ANN in the analysis of rectangular microstrip antenna on uniaxially anisotropic substrate to reduce the complexity of the spectral domain method and to minimize the CPU time necessary to obtain the numerical results. The numerical comparison between neurospectral and conventional moment methods shows significant improvements in time convergence and computational cost. Hence, the use of neurospectral approach presented here as a promising fast technique in the design of microstrip antennas.

Keywords: Microstrip antenna, Artificial neural networks, Modeling and design, Anisotropic substrate, Spectral domain analysis

Received 30 August 2015; Revised 30 December 2015; Accepted 5 January 2016; first published online 10 February 2016

I. INTRODUCTION

The increase in complexity of device modeling has led to rapid growth in the computational modeling research arena. To accommodate computational complexity, several computer-aided design (CAD) modeling engines such as artificial neural networks (ANNs) were used [1, 2]. ANNs, emulators of biological neural networks, have emerged as intelligent and powerful tools and have been widely used in signal processing, pattern recognition, and several other applications [3]. ANN is a massively parallel and distributed system traditionally used to solve problems of nonlinear computing [4].

The microstrip antenna (MSA) is an excellent radiator for many applications such as mobile antenna, aircraft and ship antennas, remote sensing, missiles, and satellite communications [5]. It consists of radiating elements (patches) photo etched on the dielectric substrate. Microstrip antennas are low-profile conformal configurations. They are lightweight, simple and inexpensive, most suited for aerospace and mobile communication. Their low-power handling capability posits these antennas better in low-power transmission and receiving applications [6]. The flexibility of the MSA to shape it in multiple ways, such as square, rectangular, circular, elliptical, triangular shapes, etc., is an added property.

Some dielectric substances exhibit anisotropy due to their natural crystal structures or as the result of their production processes [7]. Isotropic materials may also show anisotropy at high frequencies. In the design of microwave-integrated circuit components and microstrip patch antennas, anisotropic materials have been progressively popular. Especially the effects of uniaxial-type anisotropy have been investigated [7–11] due to the availability of this kind of materials such as Sapphire, Magnesium fluoride, and Epsilam-10. In these works, the physical parameters of the antenna are replaced with effective ones in order to line up the obtained theoretical results with the measured data. Although, the moment method provides better accuracy, but its computational cost is high due to the evaluation of the slowly decaying integrals and the iterative nature of the solution process. Even though all the losses can be directly included in the analysis, produced results may not provide satisfactory accuracy for all the cases [12]. Because of these problems, *Mishra* and *Patnaik* have introduced the use of neural networks in conjunction with spectral domain approach (SDA) to calculate the complex resonant frequency [13] and the input impedance of rectangular microstrip resonators [14], this approach is named the neurospectral method. In [13], the computational complexity involved in finding the complex root is reduced, whereas, in [14], the neural network method evaluates the integrals appearing in the matrix impedance. Later on Mishra and Patnaik [15] demonstrated the force of the neurospectral approach in patch antenna design using the reverse modeling

[1]Electronics Department, University of Batna, 05000 Batna, Algeria
[2]Industrial Engineering Department, University of Khenchela, 40004 Khenchela, Algeria. Phone: +21333857526
Corresponding author:
S. Bedra
Email: bedra_sami@yahoo.fr

to determine the patch dimensions for a given set of other parameters.

The objective of this work is to present an integrated approach based on ANNs and electromagnetic (EM) knowledge [8]. We introduce the artificial neural networks in the analysis of rectangular antenna to reduce the complexity of the spectral approach and to minimize the CPU time necessary to obtain the numerical results. Two points are especially emphasized; we have demonstrated the force of neurospectral approach in antenna modeling using ANN combined with EM knowledge to develop a neural network model for the calculation of resonant frequency and half-power bandwidth of rectangular patch antenna printed on isotropic or uniaxially anisotropic substrate; using reverse modeling, ANN is built to find out the antenna dimensions for the given resonant frequency, dielectric constant, and height of substrate. The ANN models are simple, easy to apply, and very useful for antenna engineers to predict both patch dimensions and resonant frequency. To the best of our knowledge, this subject has not been reported in the open literature; the only published results on modeling or design of rectangular microstrip patch resonators on isotropic substrate using neurospectral approach [13–16].

II. FORMULATION OF THE PROBLEM

The geometry under consideration is illustrated in Fig. 1. A rectangular patch with dimensions (a, b) along the two axes (x, y), respectively, is printed on a grounded dielectric slab of thickness d, characterized by the free-space permeability μ_o and the permittivity ε_o, ε_r (ε_o is the free-space permittivity and the relative permittivity ε_r can be complicated to account for dielectric loss). To simplify the analysis, the antenna feed will not be considered.

All fields and currents are time harmonic with the $e^{i\omega t}$ time dependence suppressed. The transverse fields inside the jth layer ($j = 1, 2$) can be obtained via the inverse vector Fourier transform as [17].

$$\mathbf{E}(r_s, z) = \begin{bmatrix} E_x(\mathbf{r}_s, z) \\ E_y(\mathbf{r}_s, z) \end{bmatrix} = \frac{1}{4\pi^2} \int_{-\infty}^{+\infty} \int_{-\infty}^{+\infty} \overline{\mathbf{F}}(\mathbf{k}_s, \mathbf{r}_s) \cdot \mathbf{e}(\mathbf{k}_s, z) dk_x dk_y, \quad (1)$$

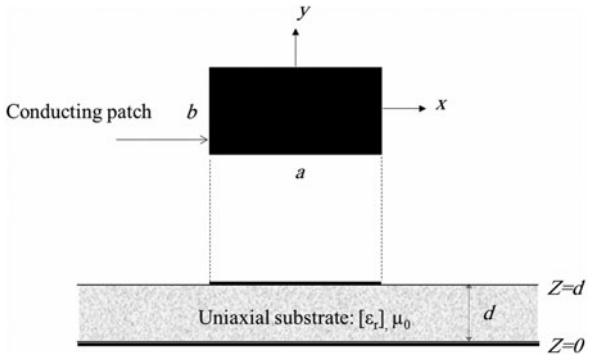

Fig. 1. Rectangular MSA structure.

$$\mathbf{H}(\mathbf{r}_s, z) = \begin{bmatrix} H_y(\mathbf{r}_s, z) \\ -H_x(\mathbf{r}_s, z) \end{bmatrix} = \frac{1}{4\pi^2} \int_{-\infty}^{+\infty} \int_{-\infty}^{+\infty} \overline{\mathbf{F}}(\mathbf{k}_s, \mathbf{r}_s) \cdot h(\mathbf{k}_s, z) dk_x dk_y, \quad (2)$$

where $\overline{\mathbf{F}}(\mathbf{k}_s, \mathbf{r}_s)$ is the kernel of the vector Fourier transform [18, 19], and

$$\mathbf{e}(\mathbf{k}_s, z) = \begin{bmatrix} \frac{\mathrm{i}}{\mathbf{k}_s} \frac{\partial \tilde{E}_z(\mathbf{k}_s, z)}{\partial z} \\ \frac{\omega \mu_o}{k_s} \tilde{H}_z(\mathbf{k}_s, z) \end{bmatrix} = \mathbf{A}(\mathbf{k}_s) e^{-\mathrm{i}\bar{\mathbf{k}}_z z} + \mathbf{B}(\mathbf{k}_s) e^{\mathrm{i}\bar{\mathbf{k}}_z z}, \quad (3)$$

$$\mathbf{h}(\mathbf{k}_s, z) = \begin{bmatrix} \frac{\omega \varepsilon_o \varepsilon_r}{\mathbf{k}_s} \tilde{E}_z(\mathbf{k}_s, z) \\ \frac{\mathrm{i}}{\mathbf{k}_s} \frac{\partial \tilde{H}_z(\mathbf{k}_s, z)}{\partial z} \end{bmatrix} = \overline{\mathbf{g}}(\mathbf{k}_s) \cdot \left[\mathbf{A}(\mathbf{k}_s) e^{-\mathrm{i}\bar{\mathbf{k}}_z z} - \mathbf{B}(\mathbf{k}_s) e^{\mathrm{i}\bar{\mathbf{k}}_z z} \right], \quad (4)$$

In equations (4) and (5), $\tilde{E}_z(\mathbf{k}_s, z)$ and $\tilde{H}_z(\mathbf{k}_s, z)$ are the scalar Fourier transforms of $E_z(\mathbf{r}_s, z)$ and $H_z(\mathbf{r}_s, z)$, respectively. **A** and **B** are two-component unknown vectors and

$$\overline{\mathbf{g}}_j(\mathbf{k}_s) = diag \left[\frac{\omega \varepsilon_o \varepsilon_{rj}}{k_z}, \frac{k_z}{\omega \mu_o} \right], \quad k_z = \left(\varepsilon_r k_o^2 - \mathbf{k}_s^2 \right) \quad (5)$$

with $k_o^2 = \omega^2 \varepsilon_o \mu_o$ and k_z is the propagation constant in the uniaxial substrate. Writing equations (4) and (5) in the planes $z = 0$ and $z = d$, and by eliminating the unknowns **A** and **B**, we obtain the matrix form

$$\begin{bmatrix} \mathbf{e}(\mathbf{k}_s, d^-) \\ \mathbf{h}(\mathbf{k}_s, d^-) \end{bmatrix} = \overline{\mathbf{T}} \cdot \begin{bmatrix} \mathbf{e}(\mathbf{k}_s, 0^+) \\ \mathbf{h}(\mathbf{k}_s, 0^+) \end{bmatrix} \quad (6)$$

with

$$\overline{\mathbf{T}} = \begin{bmatrix} \overline{\mathbf{T}}^{11} & \overline{\mathbf{T}}^{12} \\ \overline{\mathbf{T}}^{21} & \overline{\mathbf{T}}^{22} \end{bmatrix} = \begin{bmatrix} \bar{\mathbf{I}} \cos\bar{\theta} & -\mathrm{i}\bar{\mathbf{g}}^{-1} \sin\bar{\theta} \\ -\mathrm{i}\bar{\mathbf{g}} \sin\bar{\theta} & \bar{\mathbf{I}} \cos\bar{\theta} \end{bmatrix}, \quad (7)$$

which combines **e** and **h** on both sides of the jth layer as input and output quantities. In equation (8), $\boldsymbol{\theta} = \boldsymbol{k}_z d$. Now that we have the matrix representation of the anisotropic substrate characterized by the permittivity tensor, it easily to derive the dyadic Green's function of the problem in a manner very similar to that shown in [9]

$$\mathbf{e}(\mathbf{k}_s, d^-) = \mathbf{e}(\mathbf{k}_s, d^+) = \mathbf{e}(\mathbf{k}_s, d), \quad (8)$$

$$\mathbf{h}(\mathbf{k}_s, d^-) = \mathbf{h}(\mathbf{k}_s, d^+) = \mathbf{j}(\mathbf{k}_s). \quad (9)$$

$\tilde{\mathbf{J}}(\mathbf{k}_s)$ is the vector Fourier transform of current $\tilde{\mathbf{J}}(\mathbf{r}_s)$ on the patch; it accounts for the discontinuity of the tangential magnetic field at the interface $z = d$. In the unbounded air region

https://doi.org/10.1017/S1759078716000076 Published online by Cambridge University Press

above the top patch of the structure ($d\langle z\langle\infty$ *and* $\varepsilon_r = 1$), the EM field given by equations (3) and (4) should vanish at $z \to +\infty$ according to Sommerfeld's condition of radiation, this yields

$$\mathbf{h}(\mathbf{k}_s, d^+) = \bar{\mathbf{g}}_0(\mathbf{k}_s) \cdot \mathbf{e}(\mathbf{k}_s, d^+), \tag{10}$$

$$\mathbf{h}(\mathbf{k}_s, 0^-) = -\bar{\mathbf{g}}_0(\mathbf{k}_s) \cdot \mathbf{e}(\mathbf{k}_s, 0^-), \tag{11}$$

where $\bar{\mathbf{g}}_0(\mathbf{k}_s)$ can be easily obtained from the expression of $\bar{\mathbf{g}}_j(\mathbf{k}_s)$ given in equation (5) by allowing $\bar{\varepsilon}_r = 1$. The transverse electric field must necessarily be zero at the plane $z = o$, so that we have

$$\mathbf{e}(\mathbf{k}_s, d^-) = \mathbf{e}(\mathbf{k}_s, d^+) = \mathbf{e}(\mathbf{k}_s, d) = 0. \tag{12}$$

From equations (6)–(11), we obtain the following relationship:

$$\mathbf{e}(\mathbf{k}_s, d) = \bar{\mathbf{G}}(\mathbf{k}_s) \cdot \mathbf{j}(\mathbf{k}_s), \tag{13}$$

where $\bar{\mathbf{G}}(\mathbf{k}_s)$ is the dyadic Green's function in the Vector Fourier transform domain, it is given by

$$\bar{\mathbf{G}}(\mathbf{k}_s) = \left[\bar{\mathbf{T}}_1^{22}(\bar{\mathbf{T}}_1^{12})^{-1} + (\bar{\mathbf{g}}_0 \cdot \bar{\mathbf{T}}_2^{12} - \bar{\mathbf{T}}_2^{22})^{-1} + (\bar{\mathbf{g}}_0 \cdot \bar{\mathbf{T}}^{11} - \bar{\mathbf{T}}^{21})^{-1}\right]^{-1}. \tag{14}$$

Using the technique known as the moment method, with weighting modes chosen identical to the expansion modes, equations (12) and (13) are reduced to a system of linear equations which can be written compactly in matrix form [18] as

$$\bar{\mathbf{Z}} \cdot \mathbf{C} = \mathbf{o}, \tag{15}$$

where $\bar{\mathbf{Z}}$ is the impedance matrix and the elements of the vector $\mathbf{C}$ are the mode expansion coefficients to be sought [18, 19]. Note that each element of the impedance matrix $\bar{Z}$ is expressed in terms of a doubly infinite integral [18]. The system of linear equations given in equation (16) has non-trivial solutions when

$$\det[\bar{\mathbf{Z}}(\omega)] = 0. \tag{16}$$

Once the complex resonant frequency is determined, the eigenvector corresponding to the minimal eigenvalue of the impedance matrix gives the coefficients of the current on the rectangular patch. The current density is thus obtained in numerical form. This current density can be used for computing the radiation electric field in the region $z \geq d$ of Fig. 1. Using the stationary phase method [18], we can obtain the far-field pattern function on the upper air half-space of Fig. 1 in terms of the transverse electric field at the plane $z = d$ as follows:

$$\begin{bmatrix} \mathbf{E}_{\theta'}(r', \theta', \varphi') \\ \mathbf{E}_{\varphi'}(r', \theta', \varphi') \end{bmatrix} = ik_0 \frac{e^{-ik_0 r'}}{2\pi r'} \begin{bmatrix} -1 & 0 \\ 0 & \cos\theta' \end{bmatrix} \cdot \mathbf{e}(\mathbf{k}_s, d), \tag{17}$$

where $\{r', \theta', \varphi'\}$ is a local set of spherical coordinates defined with respect to the Cartesian system $\{x'' \equiv x, y' \equiv y, z' \equiv z\}$ with an origin placed at the plane $z = d$ of Fig. 1. Substituting equation (14) into (17) yields

$$\begin{bmatrix} \mathbf{E}_{\theta'}(r', \theta', \varphi') \\ \mathbf{E}_{\varphi'}(r', \theta', \varphi') \end{bmatrix} = ik_0 \frac{e^{-ik_0 r'}}{2\pi r'} \begin{bmatrix} -1 & 0 \\ 0 & \cos\theta' \end{bmatrix} \cdot \bar{\mathbf{T}}^{12} \cdot \left[\bar{\mathbf{\Gamma}}^{22} - \bar{\mathbf{g}}_0 \bar{\mathbf{\Gamma}}^{12}\right] \cdot^{-1} j(\mathbf{k}_s), \tag{18}$$

$$\bar{\mathbf{\Gamma}} = \bar{\mathbf{T}}_2 . \bar{\mathbf{T}}_1. \tag{19}$$

In equations (17) and (18), the stationary values of k_x and k_y are given by

$$k_x = -k_0 \sin\theta' \cos\varphi', \tag{20}$$

$$k_y = -k_0 \sin\theta' \sin\varphi'. \tag{21}$$

Although the full-wave analysis can give results for several resonant modes [18, 19], only results for the TM_{01} mode are presented in this study.

If we want to take the substrate uniaxial anisotropy's into account, then the number of inputs increases since the relative dielectric permittivity ε_r will be replaced by the pair of relative permittivities (ε_x, ε_z); where ε_x and ε_z are the relative dielectric permittivity along the x- and z-axes, respectively (Fig. 1). With the increase of design parameter's number, the network size increases, resulting in an increase in the size of training set required for proper generalization. Because of the different natures of the additional parameters, data generation becomes more complicated, a solution to this problem seems necessary. For the case of uniaxially anisotropic substrate, ε_{re} given in [20] their resulting values are:

$$\varepsilon_{re} = \varepsilon_z, \tag{22}$$

$$d_e = d\sqrt{\frac{\varepsilon_x}{\varepsilon_z}}. \tag{23}$$

In the next section, a basic artificial neural network is described briefly, and our application to the calculation of the resonant frequency of an MSA is then explained.

III. ANNS

ANNs have been well applied to solve many real-world problems, especially the problems that can be carefully tracked by expert systems. These systems can predict the relationship between the input and output sets without prior knowledge of the process model. The network can solve the problems related with complex engineering systems, complicated EM computation, etc. [21]. In the progression of developing an ANN model, the architecture of the neural network and the learning algorithm are the two most important factors. ANNs have many structures and structural design [19, 20]. The class of the ANN and/or the architecture selected for a particular model implementation depends on the problem to be solved.

https://doi.org/10.1017/S1759078716000076 Published online by Cambridge University Press

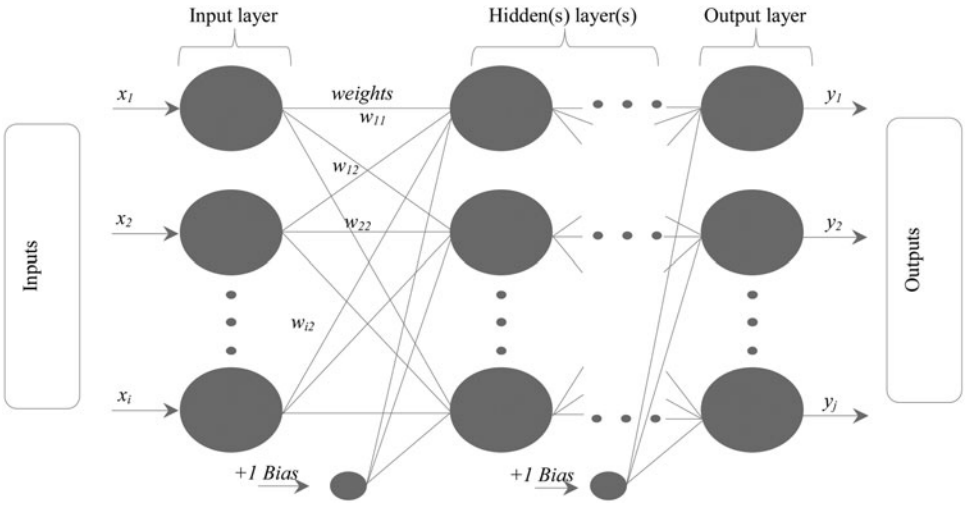

Fig. 2. General form of multilayered perceptrons.

Multilayer perceptrons (MLP) have been applied well to solve some difficult and diverse problems by training them in a supervised manner with a highly popular algorithm known as the error back-propagation algorithm [22].

As shown in Fig. 2, the MLP consists of an input layer, one or more hidden layers, and an output layer. Neurons in the layer of entry only act as buffers for distributing the input signals x_i to neurons in the hidden layer. Each neuron in the hidden layer sums its input signals x_i after weighting them with the strengths of the respective connections w_{ji} from the layer of entry and computes its output y_j as a function f of the sum, namely

$$y_j = f\left(\sum w_{ji} x_i\right), \tag{24}$$

where f can be a simple threshold function or a sigmoid or hyperbolic tangent function [23]. The output of neurons in the output layer is computed likewise.

Training of a network is accomplished through adjustment of the weights to give the desired response via the learning algorithms. An appropriate structure may still fail to provide a better model unless a suitable learning algorithm trains the structure. A learning algorithm provides the change $\Delta w_{ji}(k)$ in the weight of a connection between neurons i and j at time k. The weights are then updated according to the formula

$$w_{ji}(k+1) = w_{ji}(k) + \Delta w_{ji}(k+1). \tag{25}$$

In this work, both MLP networks were used in ANN models. MLP models were trained with almost all network learning algorithms. Hyperbolic tangent sigmoid and linear transfer functions were used in MLP training. The train and test data of the synthesis and analysis ANN were obtained from calculated with a spectral model and a computer program using the formula given in Section 2. The data are in a matrix form consisting inputs and target values and arranged according to the definitions of the problems. Using [19, 20], two are generated for learning and testing the neural model. The different network input and output parameters are shown in Fig. 3 and 4. Some stratagems are adopted to reduce time of training and ameliorate the ANN

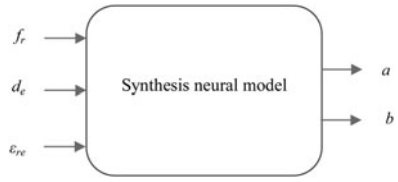

Fig. 3. Synthesis neural model for predicting the patch dimension of rectangular MSA with effective parameters.

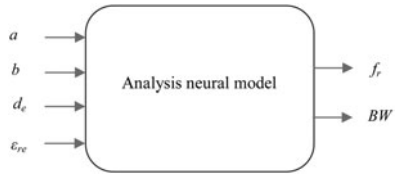

Fig. 4. Analysis neural model for calculating the resonant frequency and half-power bandwidth of rectangular MSA with effective parameters.

models correctness, such as preprocessing of inputs and output, randomizing the spreading of the learning data [24], and normalized between 0.1 and 0.9 in MATLAB software before applying training. For an applied input pattern, the arbitrary numbers between 0 and 1 are assigned to initialize the weights and biases [25]. The output of the model is then calculated for that input pattern.

The CPU time taken by the spectral domain to give the both resonant frequency and half-power bandwidth for each input set is more than half-minute; it depends on three initial values used in Muller's algorithm for not seeking of the characteristic equation. All numerical results presented in this paper we acquired on an Intel dual-core Pentium IV computer with a 2.6 GHz processor and a total RAM memory of 2 GB.

In the present paper, dimensions of the microstrip patch antenna are obtained as a function of input variables, which are height of the effective dielectric material (d_e), effective dielectric constants of the substrate (ε_{re}), and the resonant frequency (f_r), using ANN techniques (Fig. 3). Similarly, in the analysis ANN, the resonant frequency of the antenna is obtained as a function of patch dimensions (a, b), height of

https://doi.org/10.1017/S1759078716000076 Published online by Cambridge University Press

Table 1. Parameters of analysis and synthesis models.

Algorithm details	Neurospectral approach	
	Analysis model	Synthesis model
Activation function	Sigmoid	Sigmoid
Training function (back-propagation)	Trainrp	Trainrp
Number of data	380	380
Number of neurons (input layer)	4	3
Number of neurons (hidden layers)	12–8	10–8
Number of neurons (output layer)	2	2
Epochs (number of iterations)	30 000	20 000
TPE (training performance error)	10^{-4}	10^{-4}
Time required	139 min	117 min
LR (learning rate)	0.6	0. 5
MC (momentum constant)	0.7	0.7

the effective dielectric substrate (d_e), and effective dielectric constants of the material (ε_{re}) (Fig. 4). By the designer point of view, it is important to give to the calculation of the antenna physical and geometrical parameters the same importance as its resonant characteristics. Because there is no explicit model that gives the dimension of the patch directly and accurately and because of the high nonlinearity of the relationship between the resonant frequency and the patch size, the reverse modeling is needed [19]. Therefore, this example is very suitable for illustrating features and competences of synthesis ANN.

A) Forward side of the problem: the synthesis ANN

The input quantities to the ANN black-box in synthesis Fig. 3 can be ordered as:

- d_e, height of the effective dielectric substrate;
- ε_{re}, effective dielectric substrate;
- f_r, resonant frequency of the antenna.

The following quantities can be obtained from the output of the black-box as functions of the input variables:

- a, width of a rectangular patch;
- b, length of a rectangular patch.

Table 3. Comparison of the calculated bandwidth with measured and calculated data, for a rectangular microstrip patch antenna, $\varepsilon_r = 2.33$.

Input parameters (cm)			Bandwidth (%)			
			Measured	Calculated		
a	b	d	[27]	[28]	[29]	Our results
5.7	3.8	0.3175	3.12	4.98	3.5	3.17
4.55	3.05	0.3175	4.08	6.14	4.0	4.12
1.7	1.1	0.1524	6.60	8.21	4.8	6.67

Table 4. Reverse modeling (synthesis) for the prediction of antenna dimensions.

Input parameters			Target (cm)		ANN (cm)	
f_r (GHz)	d (cm)	ε_r	a	b	a	b
3.92	0.079	2.22	4	2.5	3.989	2.512
4.30	0.127	10.5	1.5	1.1	1.508	1.091
4.73	0.9525	2.33	1.7	1.1	1.698	1.114
7.87	0.1524	2.33	1.7	1.1	1.701	1.098
2.31	0.3175	2.33	5.7	3.8	5.710	3.786
4.24	0.3175	2.33	2.95	1.95	2.951	1.948
5.84	0.3175	2.33	1.95	1.3	1.948	1.304
7.70	0.3175	2.33	1.4	0.9	1.397	0.903
2.264	0.127	10.2	3	2	3.005	1.998
4.495	0.127	10.2	1.5	0.95	1.496	0.953
2.242	0.254	10.2	3	1.9	3.008	1.907

B) Reverse side of the problem: the analysis ANN

In the analysis side of the problem, terminology similar to that in the synthesis tool is used, but the resonant frequency and half-power bandwidth of the antenna are obtained from the output for a chosen effective substrate and their thickness, patch dimensions at the input side as shown in Fig. 4.

To find a proper ANN-based synthesis and analysis models for rectangular MSA printed on isotropic or uniaxially anisotropic substrate, many experiments were carried out in this study. After many trials, it was found that the target of high accuracy was summarized in Table 1.

Table 2. Analysis of computed, measured, and ANN-predicted resonant frequencies.

Substrate material	Input parameters (cm)			Resonant frequencies (GHz)			
	a	b	d	Measured [26]	Theory		Our results
					[27]	[30]	ANN
Isotropic ($\varepsilon_x = \varepsilon_z = 2.33$)	5.7	3.8	0.3175	2.31	2.32	2.46	2.32
	2.95	1.95	0.3175	4.24	4.18	4.34	4.28
	1.95	1.3	0.3175	5.84	5.86	6.01	6.00
	1.4	0.9	0.3175	7.70	7.73	7.79	7.69
Anisotropic (ε_x, ε_z) = (13.0, 10.2)	a	b	d	Measured [28]	Theory [28]	[29]	Our results ANN
	3	2	0.127	2.26	2.26	2.23	2.24
	1.5	0.95	0.127	4.49	4.52	4.47	4.53
	3	1.9	0.254	2.24	2.26	2.24	2.22

https://doi.org/10.1017/S1759078716000076 Published online by Cambridge University Press

Table 5. Comparisons of our results obtained via the proposed neurospectral model with those obtained using the conventional SDA.

Input parameters				Conventional method (SDA)			Neurospectral method		
a (cm)	b (cm)	d (cm)	ε_r	Resonant frequency (GHz)	Bandwidth (%)	CPU Time (seconds)	Resonant frequency (GHz)	Bandwidth (%)	CPU Time (s)
2.0	2.5	0.079	2.22	3.943	1.217	34.35	3.926	1.331	0.078
1.063	1.183	0.079	2.50	7.704	2.615	34.57	7.671	2.776	0.080
1.53	1.63	0.30	2.50	5.202	8.002	35.29	5.181	8.016	0.079
0.79	1.255	0.40	2.55	6.427	13.407	33.63	6.278	12.842	0.081
1.0	1.52	0.476	2.55	5.300	13.232	32.51	5.207	12.775	0.078
0.91	1.0	0.127	10.2	4.573	1.158	33.34	4.613	1.137	0.079
1.72	1.86	0.157	2.33	5.001	3.608	34.75	4.983	3.809	0.079

IV. NUMERICAL RESULTS AND DISCUSSION

In order to determine the most applicable suggestion given in the literature, we compared our computed values of the resonant frequencies of rectangular patch antennas with the theoretical and experimental results reported by other scientists [26–29], which are all given in Table 2.

From Table 3 it is observed that the bandwidths of a rectangular MSA computed by the present approach are closer to the experimental [27] and theoretical [28, 29] values.

It can be clearly seen from Tables 2 and 3 that our results calculated using the neural models proposed in this paper are better than those calculated by other scientists. The very good agreement between the measured values and our computed resonant frequency and half-power bandwidth values supports the validity of the neural model.

Table 4 gives the antenna dimension predicted by the ANN model. As it is shown, the results are in good agreement. The results of the synthesis ANN model and comparison with the targets are given in Table 4. The very good agreement between the values obtained with the model-neuronal synthesis and target values supports the validity of the neural model. The CPU time taken to calculate the patch dimensions (ground-plane apertures) using synthesis model is less than 0.079 s.

In Table 5, we compare our results obtained via the proposed neurospectral model with those obtained using the conventional spectral domain method approach (SDA). As well, to the resonant frequency and half-power bandwidth, we have also shown the CPU time in this table. It is clear that our resonant frequencies and bandwidths coincide with those obtained by the conventional moment method. Note that, the time required for obtaining the resonant frequency and half-power bandwidth using the neurospectral model is much less in comparison with the spectral domain method.

In Fig. 5, the results are presented for the resonant frequency and bandwidth of circular microstrip patch printed on an anisotropic dielectric substrate polytetrafluoroethylene (PTFE). In this figure, the results obtained for the resonant frequency and bandwidth of patch on anisotropic PTFE ($\varepsilon_x = 2.88, \varepsilon_z = 2.43$) are compared with the results that would be obtained if the anisotropy of PTFE were neglected ($\varepsilon_x = \varepsilon_z = 2.43$). The patch has dimension ($a = 1.9$ cm, $b = 2.29$ cm).

The differences between the results obtained considering anisotropy and neglecting anisotropy reach 1.61% in the case of resonant frequencies and 24.89% in the case of half-power bandwidths. Thus, it can be concluded that the effect of uniaxial anisotropy on the resonant frequency and bandwidth of a rectangular microstrip patch antenna cannot be ignored and must be taken into account in the design stage.

In Figs 6(a) and 6(b), the authors plots the radiation patterns of rectangular patch printed on isotropic ($\varepsilon_x = \varepsilon_z = 2.32$) and uniaxially anisotropic ($\varepsilon_x = 2.32, \varepsilon_z = 4.64$) substrates in both the E-plane and the H-plane. Note that the

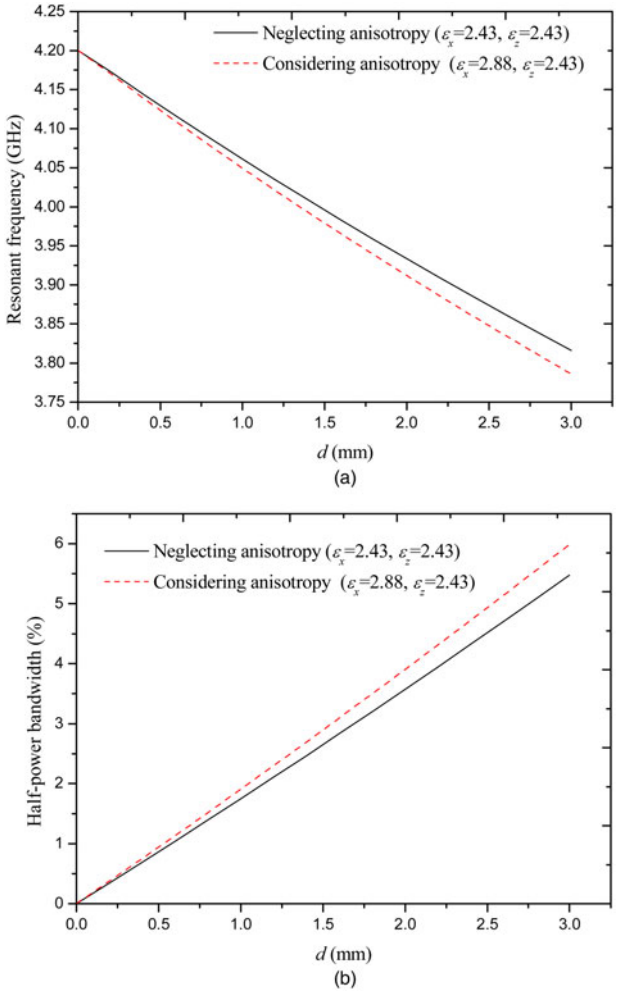

Fig. 5. Resonant frequency (a); half-power bandwidth (b) of rectangular microstrip patch printed on anisotropic PTFE substrate, the patch has a dimension of $a = 1.9$ cm, and $b = 2.29$ cm.

https://doi.org/10.1017/S1759078716000076 Published online by Cambridge University Press

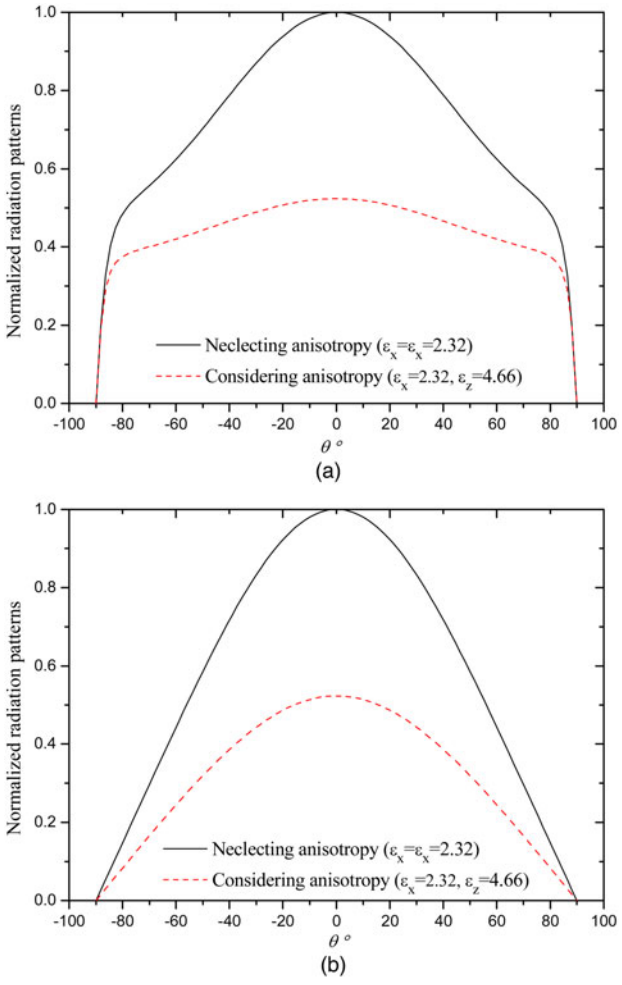

Fig. 6. Normalized radiation patterns versus the angle θ for the cases when neglecting and considering anisotropy in the substrate, (a) *E*-plane, (b) *H*-plane; with $a = 1.9$ cm, $b = 2.29$ cm, and $d = 0.159$ cm.

directivity of the antenna with ($\varepsilon_x = \varepsilon_z = 2.32$) is higher than the one with ($\varepsilon_x = 2.32$, $\varepsilon_z = 4.64$). The results show that the directivity patterns of MSA increase as the effective permittivity of the substrate decreases.

V. CONCLUSION

In this paper, a general technique is advised for modeling and design of rectangular MSA printed on uniaxially anisotropic substrates, using the SDA in conjunction with ANNs. In the design stage, synthesis is defined as the forward side and then analysis as the reverse side of the problem. During the synthesis of the antenna, it is desirable for the design engineers to know different performance parameters of an antenna simultaneously, instead of identifying individual parameters, alternatively. Hence, the present approach has been considered more generalized and efficient. The SDA combined with the ANN technique is more than a few hundred times more rapidly than the direct solution. This significant time gain makes the designing and training times negligible. Therefore, the neurospectral approach presented in this paper is an advantageous approach that can be included into a CAD implement, for the analysis, design, and optimization of practical protected Monolithic microwave integrated circuit (MMIC) devices.

ACKNOWLEDGEMENT

Authors wish to thank Pr. Djamel Benatia, Full Professor at the Department of Electronics, Batna 2 University, Algeria, for his support and help.

REFERENCES

[1] Mishra, R.K.; Patnaik, A.: Neurospectral analysis of coaxial fed rectangular patch antenna, in IEEE Antennas and Propagation Society International Symposium, Salt Lake City, UT, USA, 2000, 1062–1065.

[2] Thakare, V.V.; Singhal, P.: Microstrip antenna design using artificial neural networks. Int. J. RF Microw. Comput.-Aided Eng., **20** (1) (2010), 76–86.

[3] Devabhaktuni, V.; Mareddy, L.; Vemuru, S.; Cheruvu, V.; Goykhman, Y.; Ozdemir, T.: Sensitivity driven artificial neural network correction models for RF/microwave devices. Int. J. RF Microw. Comput.-Aided Eng., **22** (1) (2012), 30–40.

[4] Zhang, Q.-J.; Gupta, K.C.; Devabhaktuni, V.K.: Artificial neural networks for RF and microwave design-from theory to practice. IEEE Trans. Microw. Theory Tech., **51** (4) (2003), 1339–1350.

[5] Kumar, G.; Ray, K.: Broadband Microstrip Antennas, Artech House, London, 2003.

[6] Garg, R.: Microstrip Antenna Design Handbook, Artech House, Canton, 2001.

[7] Gurel, C.; Yazgan, E.: Characteristics of a circular patch microstrip antenna on uniaxially anisotropic substrate. IEEE Trans. Antennas Propag., **52** (10) (2004), 2532–2537.

[8] Bouttout, F.; Benabdelaziz, F.; Benghalia, A.; Khedrouche, D.; Fortaki, T.: Uniaxially anisotropic substrate effects on resonance of rectangular microstrip patch antenna. Electron. Lett., **35** (4) (1999), 255–256.

[9] Fortaki, T.; Benghalia, A.: Rigorous full-wave analysis of rectangular microstrip patches over ground planes with rectangular apertures in multilayered substrates that contain isotropic and uniaxial anisotropic materials. Microw. Opt. Technol. Lett., **41** (6) (2004), 496–500.

[10] Fortaki, T.; Djouane, L.; Chebara, F.; Benghalia, A.: On the dual-frequency behavior of stacked microstrip patches. IEEE Antennas Wireless Propag. Lett., **7** (2008), 310–313.

[11] Boufrioua, A.; Benghalia, A.: Radiation and resonant frequency of a resistive patch and uniaxial anisotropic substrate with entire domain and roof top functions. Eng. Anal. Bound. Elem., **32** (7) (2008), 591–596.

[12] Fortaki, T.; Khedrouche, D.; Bouttout, F.; Benghalia, A.: A numerically efficient full-wave analysis of a tunable rectangular microstrip patch. Int. J. Electron., **91** (1) (2004), 57–70.

[13] Mishra, R.; Patnaik, A.: Neurospectral computation for complex resonant frequency of microstrip resonators. IEEE Microw. Guided Wave Lett., **9** (9) (1999), 351–353.

[14] Mishra, R.; Patnaik, A.: Neurospectral computation for input impedance of rectangular microstrip antenna. Electron. Lett., **35** (20) (1999), 1691–1693.

[15] Mishra, R.K.; Patnaik, A.: Designing rectangular patch antenna using the neurospectral method. IEEE Trans. Antennas Propag., **51** (8) (2003), 1914–1921.

https://doi.org/10.1017/S1759078716000076 Published online by Cambridge University Press

[16] Bedra, S.; Benkouda, S.; Fortaki, T.: Analysis of a circular microstrip antenna on isotropic or uniaxially anisotropic substrate using neuro-spectral approach. COMPEL: Int. J. Comput. Math. Electr. Electron. Eng., **33** (1/2) (2014), 567–580.

[17] Pozar, D.M.: Microwave Engineering, Addison-Wesley, Reading, MA, 1990, 663–670.

[18] Fortaki, T.; Djouane, L.; Chebara, F.; Benghalia, A.: Radiation of a rectangular microstrip patch antenna covered with a dielectric layer. Int. J. Electron., **95** (9) (2008), 989–998.

[19] Tighilt, Y.; Bouttout, F.; Khellaf, A.: Modeling and design of printed antennas using neural networks. Int. J. RF Microw. Comput.-Aided Eng., **21** (2) (2011), 228–233.

[20] Christodoulou, C.; Georgiopoulos, M.: Applications of Neural Networks in Electromagnetics, Artechhouse, Norwood, MA, 2001.

[21] Samaddar, P.; Nandi, S.; Nandy, S.; Sarkar, D.C.; Sarkar, P.P.: Prediction of resonant frequency of a circular patch frequency selective structure using artificial neural network. Indian J. Phys., **88** (4) (2014), 397–403.

[22] Kumar, K.; Gunasekaran, N.: Bandwidth enhancement of a notch square shaped microstrip patch antenna using neural network approach, in International Conference on Emerging Trends in Electrical and Computer Technology, TN, 2011.

[23] Guney, K.; Gultekin, S.: A comparative study of neural networks for input resistance computation of electrically thin and thick rectangular microstrip antennas. J. Commun. Technol. Electron., **52** (5) (2007), 483–492.

[24] Raida, Z.: Modeling EM structures in the neural network toolbox of MATLAB. IEEE Antennas Propag. Mag., **44** (6) (2002), 46–67.

[25] Jain, S.K.; Patnaik, A.; Sinha, S.N.: Design of custom-made stacked patch antennas: a machine learning approach. Int. J. Mach. Learn. Cybern., **4** (3) (2013), 189–194.

[26] Chang, E.; Long, S.; Richards, W.: An experimental investigation of electrically thick rectangular microstrip antennas. IEEE Trans. Antennas Propag., **34** (6) (1986), 767–772.

[27] Chattopadhyay, S.; Biswas, M.; Siddiqui, J.Y.; Guha, D.: Rectangular microstrips with variable air gap and varying aspect ratio: improved formulations and experiments. Microw. Opt. Technol. Lett., **51** (1) (2009), 169–173.

[28] Pozar, D.M.: PCAAD 3.0. Personal Computer Aided Antenna Design, Antenna Design Associates, Inc, Leverett, MA, USA, 1996.

[29] Verma, A.: Input impedance of rectangular microstrip patch antenna with iso/anisopropic substrate-superstrate. IEEE Microw. Wireless Compon. Lett., **11** (11) (2001), 456–458.

[30] HFSS: High Frequency Structure Simulator, Ansoft Corp., 2009.

Lamia Barkat was born on August 03, 1991 in Batna, Algeria. She received the Master Science in Microwave and Telecommunications from University of Batna, Algeria, in 2013. She is currently with the Laboratory of Advanced Electronics at Electronics Department, University of Batna, Batna, Algeria. She is currently working toward The Ph.D. degree at the University of Batna. Her main research deals with neural network and their applications to microstrip patch antennas.

Sami Bedra was born on August 03, 1984 in Batna, Algeria. He received the Master Science and Ph.D. degrees in Electronics Engineering from University of Batna, Algeria, in 2011 and 2015, respectively. Currently, He is an Associate Professor in the Department of Industrial Engineering at Khenchela University, Algeria. He has published 15 papers in refereed journals and more than 15 papers in conference proceedings. He serves as reviewer for several technical journals. His current research activities include neural network, optimization techniques, and their applications to conducting and superconducting microstrip patch antennas.

Tarek Fortaki was born on March 31, 1972 in Constantine, Algeria. He received the Engineer of Communication degree in 1995, the Master Science degree in Microwaves in 1999, and the Doctorate degree in Microwaves in 2004, all from the Electronics Department, Faculty of Engineering Science, University of Constantine. Currently he is a Professor at the Electronics Department, Faculty of Engineering Science, University of Batna. He has published 17 papers in refereed journals and more than 40 papers in conference proceedings. He serves as reviewer for several technical journals. His main interests are electromagnetic theory, numerical methods and modeling of antennas and passive microwave circuits.

Randa Bedra was born on September 09, 1989 in Batna, Algeria. She received the Master Science in Microwave and Telecommunications from University of Batna, Algeria, in 2013. She is currently with the Laboratory of advanced electronics at Electronics Department, University of Batna, Batna, Algeria. She is currently working toward The Ph.D. degree at the University of Batna. Her main research deals with numerical methods and microstrip antennas.

https://doi.org/10.1017/S1759078716000076 Published online by Cambridge University Press